PROCEEDINGS, 51st Workshop on Geothermal Reservoir Engineering
Stanford University, Stanford, California, February 9-11, 2026
SGP-TR-230

Thermo-Mechanical Effects on Flow Channeling in Single- and Multi-Fracture Enhanced Geothermal Systems

Yujie Liu, Hui Wu*

School of Earth and Space Sciences, Peking University, Beijing, PRC 100871

*hui.wu@pku.edu.cn

Keywords: Enhanced geothermal systems, multi-scale flow channeling, multi-fracture, fracture aperture.

ABSTRACT

Flow channeling is widely recognized as a key mechanism that accelerates thermal drawdown and degrades the long-term performance of enhanced geothermal systems (EGS). In addition to fracture-scale flow channeling, non-uniform flow rate allocation among fractures induced from wellbore-induced pressure loss and thermo-mechanical interactions between fractures can further complicate flow behavior in multi-fracture EGSs. To systematically investigate these coupled effects, we develop field-scale single- and double-fracture EGS models and simulate the fully coupled thermo-hydro-mechanical (THM) processes. Numerical simulations first reveal how injection flow rate governs thermo-mechanical responses and flow channeling within a single fracture. Low injection flow rates lead to localized cooling, strong thermal stress accumulation, and pronounced aperture heterogeneity, resulting in severe flow channeling. In contrast, high injection flow rates generate a broader cooling zone and reduce fracture stiffness over a larger area, producing more spatially distributed aperture evolution and relatively uniform fracture flow, despite faster thermal drawdown. Extending to the double-fracture system, wellbore pressure loss induces persistent asymmetric flow allocation, producing flow behavior in each fracture similar to that in single-fracture cases, while overlapping thermal perturbation zones between closely spaced fractures create strong inter-fracture thermo-mechanical coupling, synchronizing aperture evolution and enhancing flow redistribution.

1. INTRODUCTION

High-temperature geothermal energy stored in hot dry rocks (HDR) has long been recognized as a promising source of clean and sustainable energy (Brown et al., 2021; Olasolo et al., 2016; Tester et al., 2006). However, HDR is typically located in deep subsurface formations (generally deeper than 3 km) and is characterized by extremely low permeability and porosity, which poses substantial challenges for efficient geothermal energy extraction. To overcome these limitations, enhanced geothermal systems (EGS) have been proposed as an effective approach for improving heat extraction and enabling commercial-scale power generation (Gong et al., 2023; Lu et al., 2018; Olasoloe et al., 2016). In EGS, fluid flow and heat transport within artificial and natural fracture networks play a dominant role in controlling the overall heat extraction performance.

During heat extraction, the injected working fluid does not flow uniformly through the entire fracture network. Instead, it preferentially migrates along high-permeability fractures or dominant flow channels, concentrating within limited regions between the injection and production wells. This behavior is commonly referred to as flow channeling (Fu et al., 2016; Guo et al., 2016). With the advancement of hydraulic stimulation technologies, multi-fracture systems can be created in EGS, making flow channeling a multiscale phenomenon. At the scale of a single fracture, the concentration of fluid flow within a few localized channels is known as intra-fracture flow channeling (Gee et al., 2021; Guo et al., 2016; McLean and Espinoza, 2023). At the scale of fracture networks, fluid may preferentially flow through only a few fractures or even a single dominant fracture, which is referred to as inter-fracture flow channeling (Gee et al., 2021; McLean and Espinoza, 2023; Slatlem Vik et al., 2018).

Flow channeling originates from an uneven flow distribution established at the early stage of heat extraction. This initial imbalance mainly results from fracture aperture heterogeneity, which induces spatial variations in permeability and causes the injecting fluid to preferentially migrate along high-permeability pathways connecting injection and production wells (Fox et al., 2015; Guo et al., 2016; Liu et al., 2024; Tsang and Neretnieks., 1998). As heat extraction proceeds, thermally induced aperture variations further exacerbate flow channeling. Continuous circulation of cold water cools the surrounding rock, generating thermal stresses that induce rock contraction and promote fracture opening (Fox et al., 2015; Guo et al., 2016). Importantly, since regions with initially higher flow rates experience more pronounced cooling, aperture enlargement is further amplified in these zones, leading to increasingly heterogeneous aperture distributions. This positive feedback mechanism progressively intensifies flow localization and results in a growing concentration of fluid within a limited portion of the fracture (Liu et al., 2024; 2026). In multi-fracture systems, this behavior is further complicated by pressure losses in the connecting wellbore, which introduce unequal inlet pressures among individual fractures and thereby modify the initial flow distribution (Asai et al., 2022; Gee et al., 2021; McLean and Espinoza, 2023). Moreover, since thermal contraction can accumulate between adjacent fracture planes, the degree of flow channeling is further aggravated in such systems (Slatlem Vik et al., 2018). Consequently, intra- and inter-fracture channeling can coexist in a multi-fracture EGS, significantly reducing the effective flow and heat exchange area and thereby deteriorating the overall heat extraction performance. It is also worth noting that inter-fracture flow channeling diminishes in high-stress reservoirs, as large compressive contact stresses reduce fracture compressibility and inhibit substantial fracture opening (Gee et al., 2021; McLean and Espinoza, 2023).

Although previous studies have investigated fracture aperture evolution and multiscale flow channeling, the mechanisms governing their coupled behavior under different injection flow rates remain insufficiently understood. In particular, variations in injection flow rate control the spatial extent and magnitude of thermally induced aperture changes, which in turn influence the emergence and intensity of flow channeling within individual fractures. Understanding these single-fracture responses is crucial, as they provide the foundation for interpreting flow redistribution in multi-fracture EGSs, where wellbore pressure losses and thermo-mechanical interactions naturally induce non-uniform flow allocation among fractures.

In the present study, we first examine flow channeling at the single-fracture scale by analyzing fracture aperture evolution under different injection flow rates, with particular emphasis on the associated variations in fracture hydraulic conductivity and intra-fracture flow channeling. The analysis is then extended to a double-fracture system, in which differences in flow rates among individual fractures emerge naturally due to wellbore pressure losses rather than being prescribed. Based on this framework, both intra- and inter-fracture flow channeling in multi-fracture systems are systematically evaluated. We develop a field-scale EGS model incorporating two vertical fractures and coupled injection and production wellbores to simulate the coupled thermo-hydro-mechanical (THM) processes. In the following sections, we first introduce the coupled THM model with the consideration of wellbore effect in section 2. Section 3 introduces the EGS model, including model geometries, initial and boundary conditions. Section 4 discusses the numerical results, focusing on fracture aperture evolution and hydraulic response under different prescribed injection flow rates at the single-fracture scale, and then on the resulting flow redistribution and channeling behavior in the multi-fracture system.

2. COUPLED THM MODEL INCORPORATING WELLBORE EFFECTS

We use GEOS, an open source, multi-physics coupled numerical platform developed at the Lawrence Livermore National Laboratory (LLNL), to simulate the coupled THM processes incorporating the wellbore pressure loss (Settgast et al., 2024). The numerical algorithms of coupled THM processes have been introduced clearly in previous studies and are therefore not repeated here (Guo et al., 2016; Liu et al.,2026).

In order to evaluate the effect of wellbore pressure loss on injection flow rate allocation and therefore flow behavior of individual fracture, we incorporate virtual wellbore in our model using Darcy-Weisbach equation,

$$\frac{\Delta p}{L} = f_{\mathrm{D}} \frac{\rho}{2} \frac{v^2}{D} \tag{1}$$

Where Δp is wellbore pressure loss, L is distance between two fractures, f_{D} is friction factor, ρ is fluid density, v is average flow velocity in wellbore, and D is the hydraulic diameter of wellbore. In our model, the friction factor f_{D} is determined according to the flow regime characterized by the Reynolds number (R_{e}) (Asai et al, 2022; Gee et al., 2021). The Reynolds number is computed based on the instantaneous fluid properties and flow velocity, allowing the friction factor to vary dynamically with changing injection conditions,

$$R_{\mathrm{e}} = \frac{\rho v D}{\mu} \tag{2}$$

Where μ is fluid viscosity. For laminar flow ($R_{\mathrm{e}} < 2000$), the friction factor is calculated analytically as,

$$f_{\mathrm{D}} = \frac{64}{R_{\mathrm{e}}} \tag{3}$$

For transitional and turbulent flow ($R\mathrm{e} \geq 4000$), the friction factor depends on both the Reynolds number and the relative roughness of the wellbore wall. In this case, f is evaluated using the explicit Haaland equation,

$$\frac{1}{\sqrt{f_{\mathrm{D}}}} = -1.8 \log_{10} \left[\left(\frac{\varepsilon}{3.7D} \right)^{1.11} + \frac{6.9}{R_{\mathrm{e}}} \right] \tag{4}$$

where ε is the absolute roughness of the wellbore wall. In the transitionary phase between laminar and turbulent flow, $2000 \leq R_{\mathrm{e}} \leq 4000$, the friction factor is linearly interpolated between f_{D} ($R_{\mathrm{e}} = 2000$) and f_{D} ($R_{\mathrm{e}} = 4000$) (Gee et al., 2021).

We adopt a sequential coupling approach for the THM and wellbore models, divided into four main steps: First, at each timestep, the total injection flow rate is initially divided equally between the fractures. Based on this provisional flow allocation, the TH solver computes the fluid pressure and temperature in each fracture element by solving the mass and energy conservation equations using the finite volume method (FVM). The resulting fracture pressure fields are then passed to a wellbore flow solver, where pressure losses along the injection and production wellbores are evaluated. By enforcing pressure balance along different wellbore-fracture flow paths, the injection flow rate allocated to each fracture is iteratively updated. Second, the converged fracture flow rates are subsequently fed back into the TH solver to update the fracture pressure and temperature fields. Third, the converged pressure and temperature distributions at each timestep are fed into the mechanical solver to update the stress field in the model. Thermal stresses induced by rock cooling are explicitly considered, and the effective stress is obtained by solving the deformation equilibrium equations using the finite element method (FEM). Finally, the fracture aperture is updated as a function of effective normal stress following the formulation proposed by Guo et al. (2016),

$$A = A_{\max} - \frac{a\sigma_{\mathrm{n}}}{1 + b\sigma_{\mathrm{n}}} \tag{5}$$

where A_{max} is the aperture at zero effective normal stress, and σ_n is the effective normal stress acting on the fracture. The model parameters a and b are determined from two prescribed reference stress-aperture pairs $(\sigma_{n,r1}, A_{r1})$ and $(\sigma_{n,r2}, A_{r2})$ using the following expressions,

$$a = \frac{A_{r1}A_{r2}(A_{r2} - A_{r1})(\sigma_{n,r1} - \sigma_{n,r2})}{(\sigma_{n,r1}A_{r1} - \sigma_{n,r2}A_{r2})^2} \tag{6}$$

$$b = \frac{A_{r2} - A_{r1}}{\sigma_{n,r1}A_{r1} - \sigma_{n,r2}A_{r2}} \tag{7}$$

In the present study, the first reference state is defined by an initial effective normal stress of 8 MPa and a corresponding aperture of 3 cm, while the second reference state corresponds to an effective normal stress of 1.33 MPa and an aperture of 12 cm. These values are consistent with the evolution characteristics of fractures in reservoirs with relatively low *in-situ* stresses. The updated apertures are then used in the subsequent timestep to re-evaluate fracture flow and heat transfer.

3. FIELD-SCALE SINGLE-FRACTURE AND DOUBLE-FRACTURE EGS MODELS

Two field-scale EGS models are developed, representing single-fracture and double-fracture configurations, respectively, each with dimensions of 3000 × 3000 × 3000 m³ (Figure 1). In the single-fracture model, a vertical circular fracture with a diameter of 1000 m is positioned at the center of the domain and hydraulically connects an injection well and a production well separated by a distance of 500 m. The fracture is discretized using elements with a size of 10 × 10 × 0.004 m³, while the surrounding rock matrix adjacent to the fracture is discretized into hexahedral elements with a size of 10 × 10 × 10 m³. To ensure computational efficiency, the mesh resolution is gradually coarsened toward the far field, where element sizes increase to a maximum of 300 × 300 × 500 m³. In the double-fracture model, two vertical fractures are embedded within the domain, while the remaining geometric configuration and discretization strategy are kept consistent with those of the single-fracture model.

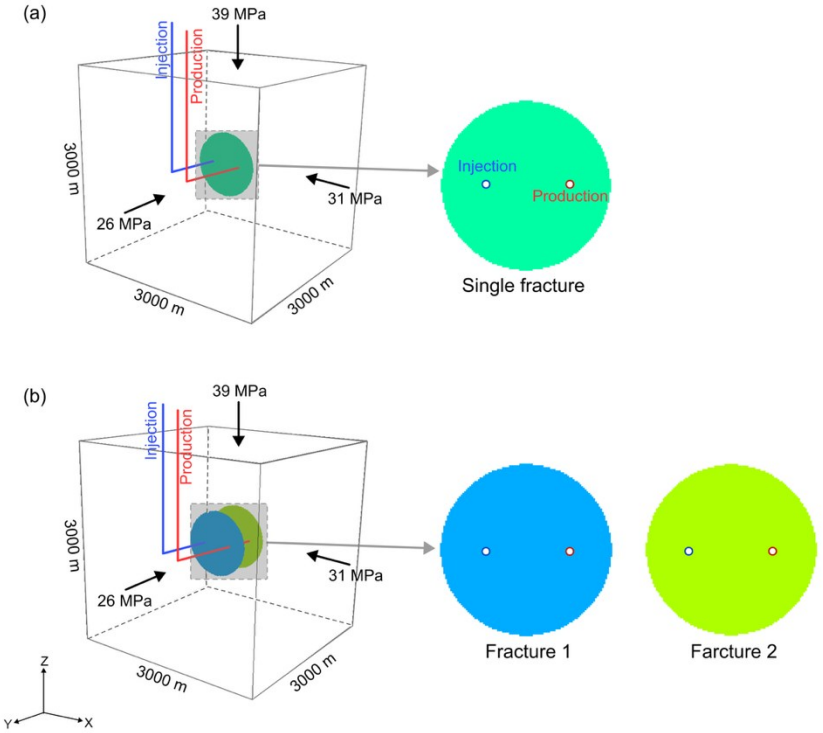

Figure 1: Sketch of field-scale EGS models. (a) single-fracture EGS model. (b) double-fracture EGS model. Note that the injected fluid initially flows through fracture 1 and then through fracture 2.

In the simulations, the reservoir is assumed to have uniform *in-situ* stress and initial temperature. The *in-situ* stress components are 31 MPa in the *x*-direction, 26 MPa in the *y*-direction, and 39 MPa in the *z*-direction, consistent with conditions of Gee et al. (2021). The initial reservoir temperature is set to 200 °C, and the circulating fluid is injected into the fracture at a temperature of 50 °C. For the single-fracture model, injection flow rates of 10 and 40 kg/s are considered, whereas a total injection flow rate of 50 kg/s is prescribed for the double-fracture model. All fractures are assigned a homogeneous initial aperture of 3 mm and permeability of 5.67×10^{-7} m^2 (Figure 1). The downhole pressure at the production well is maintained at 18 MPa throughout the simulation period. All external boundaries of the model are impermeable to fluid flow and heat transfer, while mechanical boundary conditions are specified by imposing zero normal displacement on one boundary face in each principal direction and applying the prescribed in-situ stresses on the opposite faces. The major physical properties of the rock matrix used in the model are summarized in Table 1.

Table 1: Rock matrix properties of this model.

Parameter	Value	Parameter	Value
Porosity	0.01	Density	2500 kg/m^3
Permeability	1×10^{-18} m^2	Special heat capacity	790 J/kg/K
Shear modulus	20 GPa	Thermal conductivity	3.05 W/m/K
Bulk modulus	33.3 GPa	Thermal expansion coefficient	3×10^{-6} K^{-1}

4. SIMULATION RESULTS

4.1 Single-fracture response under low- and high-injection flow rates

In this subsection, we present simulation results to illustrate the stress response, fracture aperture evolution, and the associated flow and heat transfer behavior under different injection flow rates. We first examine two representative cases, 10 kg/s and 40 kg/s, to contrast the mechanical and hydraulic responses of the fracture under low- and high-injection conditions, with particular attention to the evolution of stress state and fracture aperture. The analysis is then extended to compare the resulting variations in fracture hydraulic conductivity, flow distribution, and heat transfer behavior across different injection conditions.

We use $\Delta\boldsymbol{\sigma}'$ and $\Delta\boldsymbol{A}$ to represent the changes in effective normal stress and fracture aperture relative to their initial states respectively, which are calculated as,

$$\Delta\boldsymbol{\sigma}' = \boldsymbol{\sigma}' - \boldsymbol{\sigma}'_0 \tag{8}$$

$$\Delta A = A - A_0 \tag{9}$$

where $\boldsymbol{\sigma}'$ and A denote the effective normal stress and fracture aperture at the current simulation time, respectively, and $\boldsymbol{\sigma}'_0$ and A_0 are their corresponding initial values. Positive values of $\Delta\boldsymbol{\sigma}'$ and ΔA indicate increases in effective normal stress and fracture aperture, respectively, relative to their initial states.

4.1.1 Aperture variation under low injection flow rate

Under the low injection flow rate condition, the development of thermal stress is closely linked to the evolution of fracture stiffness. Since fluid circulation and thermal perturbation remain spatially localized and progress slowly at the low flow rate, the fracture experiences limited aperture opening during the early stage of cooling. Accordingly, the fracture maintains a relatively high normal stiffness and exhibits reduced mechanical compliance to thermally induced deformation. Consequently, the cooling-induced contraction of the surrounding rock cannot be effectively accommodated by fracture opening and is instead translated into thermal stress accumulation (first row of Figure 2). In addition, the pore pressure change in the fracture is ignorable due to the relatively large initial aperture. Therefore, under the combined effect of accumulated thermal stress and pore pressure support, the effective normal stress within the flow area decreases overall and falls below zero near the injection well (second row of Figure 2). This reduction in effective normal stress promotes substantial fracture aperture changes, manifesting as pronounced local fracture opening (third row of Figure 2).

It is noteworthy that a circular region outside the cooling zone experiences a reduction in thermal stress due to stress redistribution, which increases the effective normal stress in this area (first and second rows of Figure 2). Consequently, the fracture aperture here decreases below its initial value (third row of Figure 2). Moving farther from the flow area, the stress and aperture gradually approach the initial states. Such an enhanced aperture non-uniformity further induces significant stress redistribution within the fracture system.

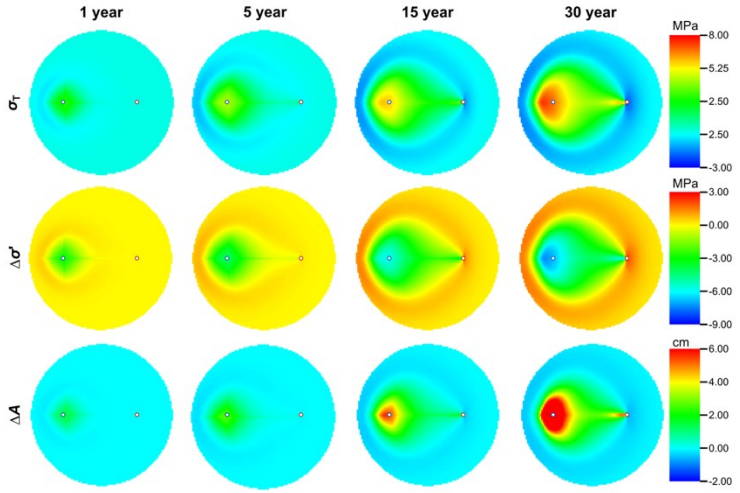

Figure 2: Evolution in thermal stress (σ_T), effective normal stress change ($\Delta\sigma'$) and fracture aperture change (ΔA) over 30 years of heat extraction at an injection flow rate of 10 kg/s.

4.1.2 Aperture variation under high injection flow rate

Under the high injection flow rate condition, the injected cold fluid rapidly establishes a large cooling zone within the fracture, inducing thermal stress in the surrounding rock through heat exchange. However, unlike the low flow rate case, the fracture here exhibits a more significant reduction in normal stiffness due to a larger aperture variation area, meaning its mechanical constraint against thermally induced deformation is lower. As a result, although the temperature decreases faster under the high flow rate, the amplitude of local aperture increase is smaller than that observed under the low flow rate (first row of Figure 3). Correspondingly, the reduction in effective normal stress within the cooling zone is less pronounced, resulting in a widespread but moderate increase in fracture aperture, and the overall aperture variation tends to remain relatively uniform (second and third rows of Figure 3).

In this scenario, the large aperture variation area induced by the high flow rate leads to stress redistribution primarily near the fracture edges and close to the production well (first and second rows of Figure 3). Notably, the region with the maximum fracture aperture does not coincide with the injection well, where the temperature drop is most pronounced. Instead, it is concentrated on the left side of the injection well, as the mechanical constraint near the well is lower than that at the left fracture boundary (Figure 3). Consequently, the fracture can accommodate more deformation in this less constrained region, even though the local thermal stress magnitude is comparable.

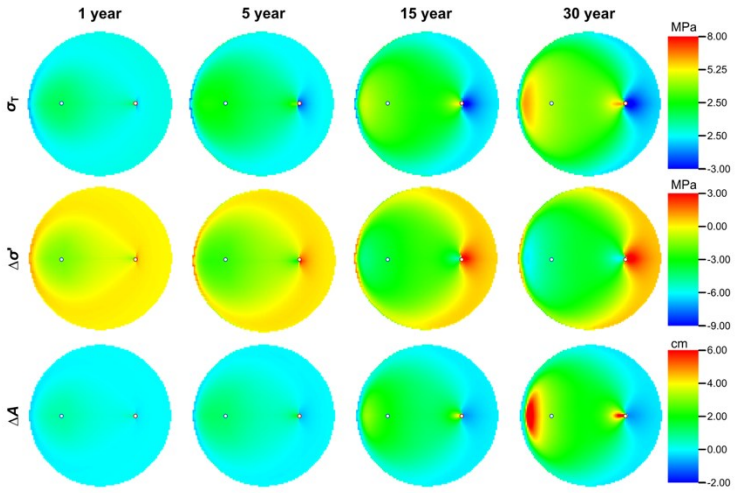

Figure 3: Evolution in thermal stress (σ_T), effective normal stress change ($\Delta\sigma'$) and fracture aperture change (ΔA) over 30 years of heat extraction at an injection flow rate of 40 kg/s.

4.1.3 Flow channeling behavior comparison

Under the low injection flow rate condition, the initial flow area within the fracture is limited due to the slow fluid circulation. Combined with the reduction of fracture aperture in the surrounding circular region caused by stress redistribution, fluid flow becomes progressively confined to a few high-aperture zones. This leads to pronounced flow channeling and small heat transfer area under low flow rate

conditions (Figure 4). In contrast, under high injection flow rate, fluid flow is more widespread and less constrained by low-aperture regions, resulting in a larger effective heat exchange area (Figure 4).

To quantify the fracture's flow efficiency under different injection rates, we further analyzed the hydraulic resistance within the fracture. Higher hydraulic resistance indicates lower hydraulic conductivity. Under the low injection flow rate condition, flow is more localized, leading to higher equivalent hydraulic conductivity compared with the high flow rate case (Figure 5). This demonstrates that the fracture's hydraulic performance cannot be simply inferred from the magnitude of the injection flow rate.

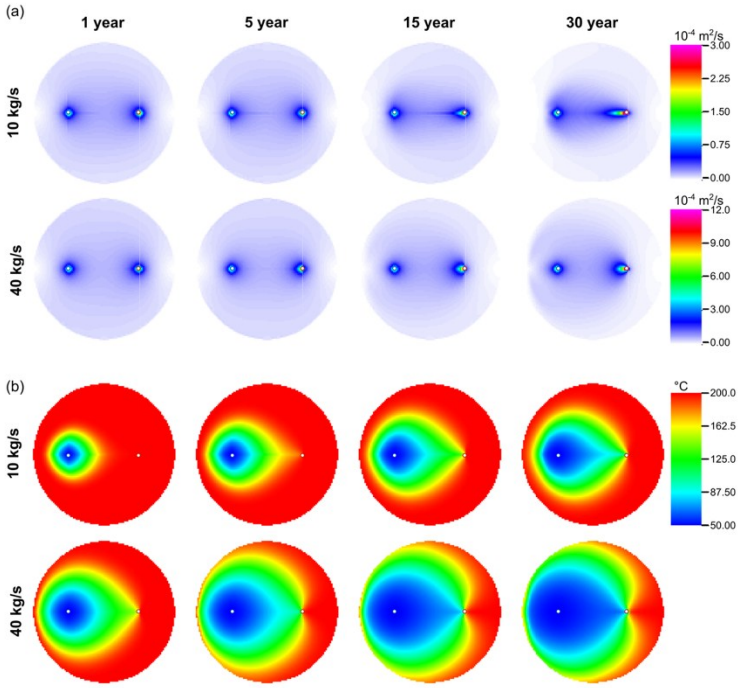

Figure 4: Evolution in (a) flow rate and (b) temperature over 30 years of heat extraction at the injection flow rates of 10 and 40 kg/s, respectively.

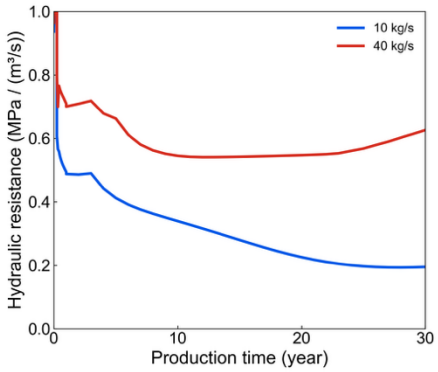

Figure 5: Fracture hydraulic resistance curves under the injection flow rates of 10 and 40 kg/s, respectively.

4.2 Double-fracture response to wellbore pressure loss and fracture interaction

We consider two vertical fractures with a spacing of 500 m to investigate the influence of wellbore pressure loss on flow distribution. To further examine the effect of fracture thermo-mechanical interaction on flow behavior, results for a smaller spacing of 100 m are also presented. In both cases, the fractures share identical initial geometric and hydraulic properties, such that any observed differences in flow partitioning arise solely from wellbore effects and inter-fracture interactions.

4.2.1 Wellbore pressure loss effects on double-fracture behavior

For a large spacing double-fracture system, the system behavior is primarily governed by pressure losses along the wellbore. As fluid flows downward within the injection well, cumulative pressure loss results in a lower inlet pressure for fracture 2 compared with the first

one. Consequently, even with identical initial fracture properties, the system naturally develops an asymmetric flow distribution, with the fracture 1 consistently receiving a higher injection rate than the fracture 2 (Figure 6(a)).

Within the double-fracture system, fracture aperture evolution exhibits a flow-rate-dependent behavior similar to that observed in the single-fracture case. Under high injection flow rates, aperture variations extend over a broader spatial region, whereas under low flow rates, aperture changes are characterized by larger local magnitudes (Figure 6(b)). From the perspective of fracture flow properties, the second fracture maintains a slightly lower hydraulic resistance (Figure 7(a)). However, when the additional hydraulic resistance introduced by pressure losses in both the injection and production wellbores is taken into account, the overall flow resistance associated with the second fracture becomes larger than that of the first fracture (Figure 7(a)). As a result, the fracture 1 retains a higher flow rate throughout the entire heat extraction period. Nevertheless, the difference in flow between the two fractures remains minor because the variations in overall hydraulic resistance are small, limiting significant redistribution of the injection flow (Figure 7(b)).

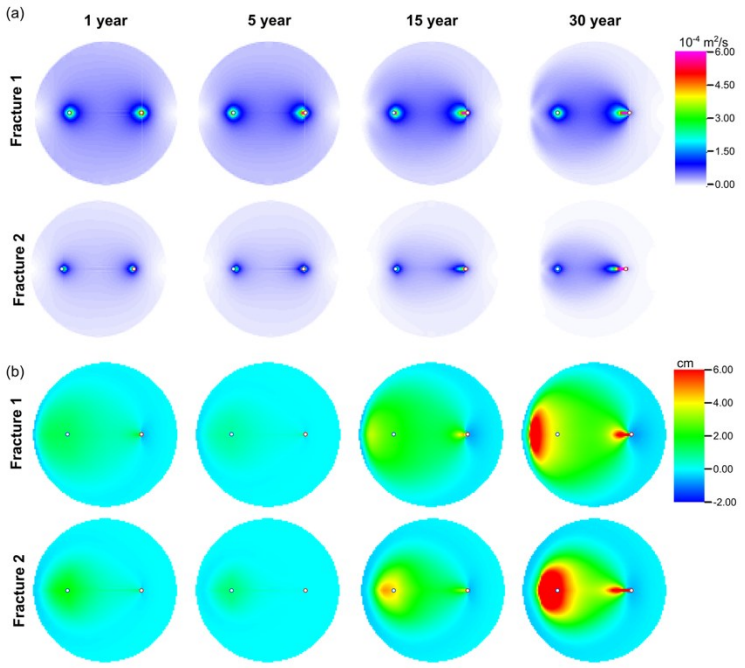

Figure 6: Evolution in (a) flow rate and (b) fracture aperture change (ΔA) over 30 years of heat extraction of the two fractures.

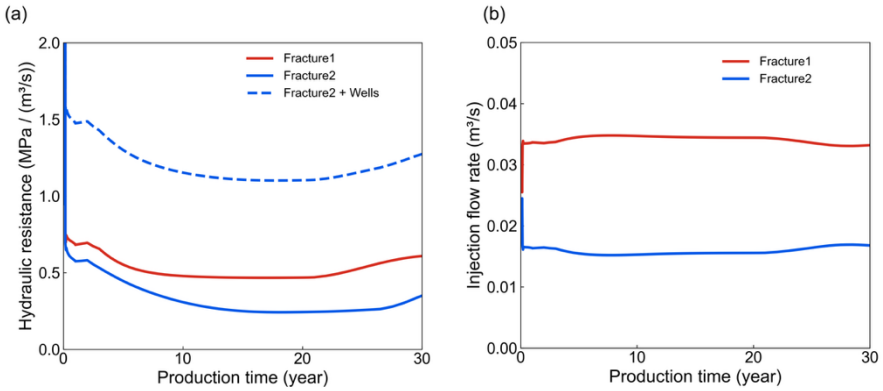

Figure 7: (a) Hydraulic resistance and (b) injection flow rate curves of the two fractures, including the effects of wellbore pressure loss.

4.2.2 Fracture interaction effects on double-fracture behavior

When the fracture spacing is reduced to 100 m, the first fracture continues to receive a higher flow rate than the second fracture. However, the difference in flow allocation between the two fractures becomes smaller than in the large-spacing case (Figure 8(a)). This reduction arises from the diminished relative influence of wellbore pressure loss as the two fractures become closer in depth.

In contrast to the large-spacing configuration, thermo-mechanical interactions between the two fractures play a significant role in the small-spacing case. As cold fluid circulates through the fractures, the surrounding rock temperature gradually decreases, inducing thermal

contraction and generating substantial thermal stress. Due to the proximity of the two fractures, their temperature perturbation zones overlap, creating a pronounced thermal-mechanical coupling effect in the region between the fractures. This coupling leads to a significant reduction in effective normal stress around the fractures, especially in the inter-fracture region (Figure 9), which simultaneously promotes pronounced fracture opening. Compared with the single-fracture and large-spacing cases, the apertures of both fractures exhibit more pronounced and synchronized evolution under strong thermo-mechanical coupling (Fig. 8(b)). In addition, the similarity in the thermal and stress environments leads to nearly identical aperture evolution patterns, which in turn result in comparable hydraulic resistance for the two fractures (Figure 10(a)). Nevertheless, when wellbore-induced pressure losses are incorporated into the overall flow path, the second fracture remains associated with a higher total hydraulic resistance, causing the first fracture to maintain a higher flow rate throughout the heat extraction process (Figure 10).

It is noteworthy that the intensified aperture evolution driven by fracture interaction produces more pronounced variations in hydraulic resistance, leading to a larger degree of flow redistribution compared with the large-spacing case. Although the absolute magnitude of flow rate variation remains limited, with a maximum change of approximately 4 kg/s, the enhanced sensitivity of flow partitioning clearly reflects the influence of thermo-mechanical coupling between closely spaced fractures (Figure 10(a)).

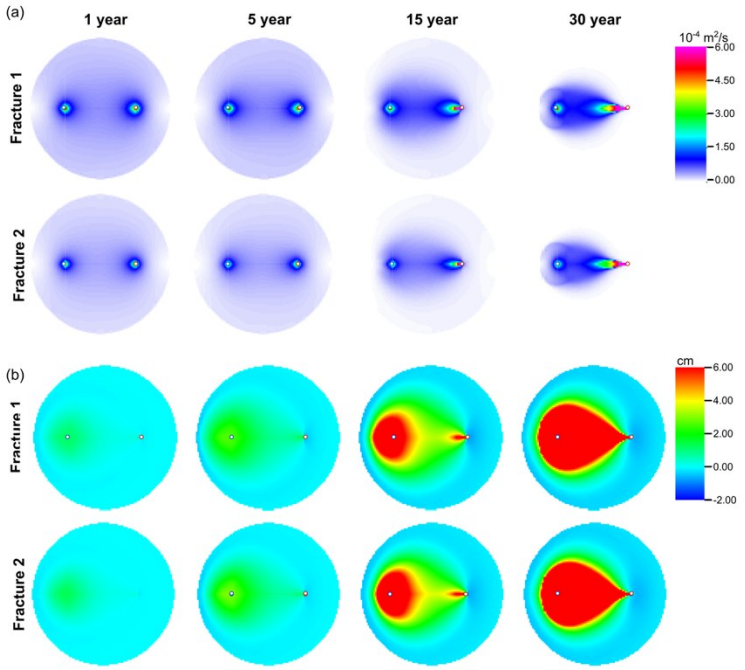

Figure 8: Evolution in (a) flow rate and (b) fracture aperture change (ΔA) over 30 years of heat extraction of the two fractures for the 100 m fracture spacing case.

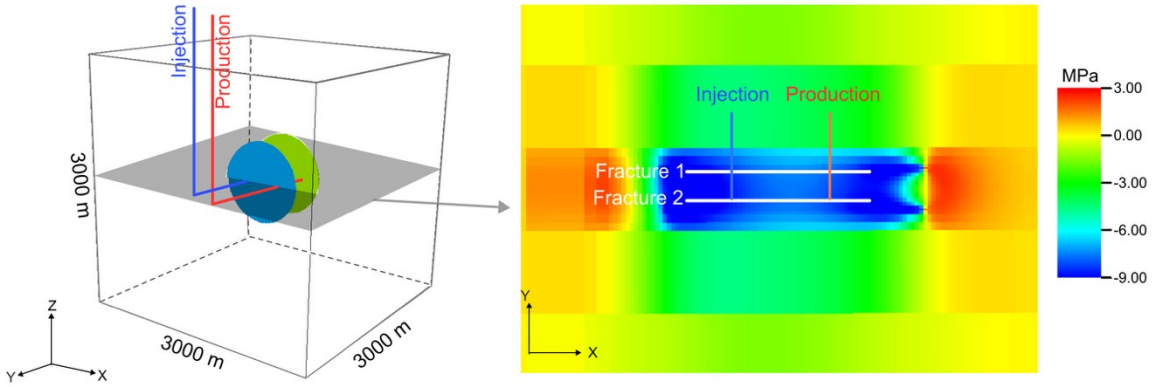

Figure 9: Spatial distribution of effective normal stress change ($\Delta\sigma'$) in the rock matrix on a horizontal cross-section at 30 years.

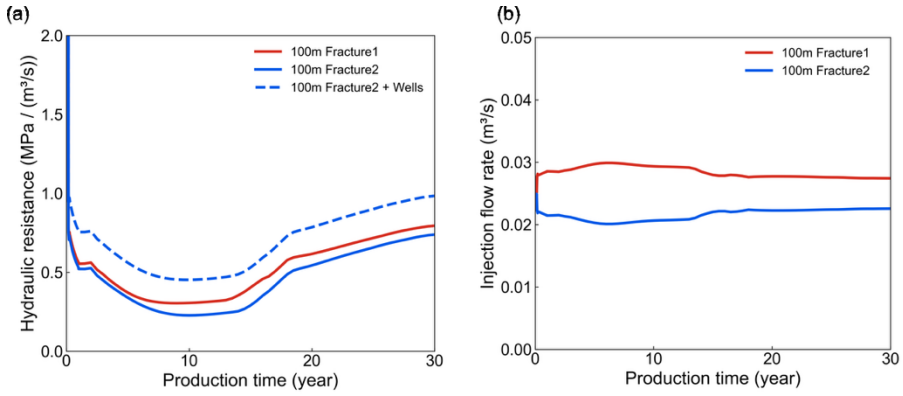

Figure 10: (a) Hydraulic resistance and (b) injection flow rate curves of the two fractures for the 100 m fracture spacing case, including the effects of wellbore pressure loss.

5. CONCLUSIONS

We quantitatively investigated the coupled thermo-mechanical effects on fracture aperture evolution and flow channeling in field-scale EGS models with single- and double-fracture configurations, explicitly accounting for wellbore pressure losses.

At low injection flow rates, localized cooling leads to strong thermal stress accumulation, resulting in pronounced local fracture opening and severe flow channeling. In addition, stress redistribution induces a surrounding annular zone with increased effective normal stress, which further constrains flow spreading and enhances flow channeling. In contrast, high injection flow rates generate a broader cooling zone and reduce fracture stiffness over a larger area, producing more spatially distributed aperture evolution and relatively uniform fracture flow. As a result, although thermal drawdown occurs more rapidly under high flow rates, the degree of flow channeling is weaker than that under low flow rate conditions.

For double-fracture systems, wellbore pressure loss introduces an inherent asymmetry in flow partitioning, causing the upper fracture to consistently receive a higher injection rate even when fractures have identical initial properties. When fracture spacing is large, flow redistribution is primarily governed by wellbore pressure losses, and thermo-mechanical interaction between fractures remains weak. When fracture spacing is reduced, overlapping thermal perturbation zones induce strong thermo-mechanical coupling, leading to synchronized aperture evolution and flow behavior. Nevertheless, wellbore-induced pressure losses remain the dominant control on inter-fracture flow allocation.

REFERENCES

Brown, D. W., Duchane, D. V., Heiken, G., Hriscu, V. T.: Mining the earth's heat: hot dry rock geothermal energy. Springer Science & Business Media, (2012).

Olasolo, P., Juárez, M. C., Morales, M. P., Damico, S., Liarte, I. A. Enhanced geothermal systems (EGS): A review. Renewable and Sustainable Energy Reviews, 56, (2016), 133-144.

Tester, J. W., Anderson, B. J., Batchelor, A. S., Blackwell, D. D., DiPippo, R., Drake, E. M., et al. The future of geothermal energy. Massachusetts Institute of Technology, 358, (2006), 1-3.

Gong, L., Han, D., Chen, Z., Wang, D., Jiao, K., Zhang, X., et al. Research status and development trend of key technologies for enhanced geothermal systems. Natural Gas Industry B, 10(2), (2023), 140-164.

Lu, S. M. A global review of enhanced geothermal system (EGS). Renewable and Sustainable Energy Reviews, 81, (2018), 2902-2921.

Fu, P., Hao, Y., Walsh, S. D. C., Carrigan, C. R. Thermal Drawdown-Induced Flow Channeling in Fractured Geothermal Reservoirs. Rock Mechanics and Rock Engineering, 49(3), (2016) 1001-1024.

Guo, B., Fu, P., Hao, Y., Peters, C. A., Carrigan, C. R. Thermal drawdown-induced flow channeling in a single fracture in EGS. Geothermics, 61, (2016), 46-62.

Gee, B., Gracie, R., Dusseault, M. B. Multiscale short-circuiting mechanisms in multiple fracture enhanced geothermal systems. Geothermics, 94, (2021).

McLean, M. L., Espinoza, D. N. Thermal destressing: Implications for short-circuiting in enhanced geothermal systems. Renewable Energy, 202, (2023), 736-755.

Slatlem Vik, H., Salimzadeh, S., Nick, H. M. Heat recovery from multiple-fracture enhanced geothermal systems: The effect of thermoelastic fracture interactions. Renewable Energy, (2018), 121, 606-622.

Fox, D. B., Koch, D. L., Tester, J. W. The effect of spatial aperture variations on the thermal performance of discretely fractured geothermal reservoirs. Geothermal Energy, 3(1), (2015), 1-29.

Tsang, C. F., Neretnieks, I. Flow channeling in heterogeneous fractured rocks. Reviews of Geophysics, 36(2), (1998), 275-298.

Liu, Y., Wu, H., Taleghani, A. D., Zhang, K., Zhang, J., Yang, M., et al. Effects of temperature-dependent viscosity on thermal drawdown-induced fracture flow channeling in enhanced geothermal systems. Renewable Energy, 235, (2024), 121274.

Asai, P., Podgorney, R., McLennan, J., Deo, M., Moore, J. Analytical model for fluid flow distribution in an Enhanced Geothermal Systems (EGS). Renewable Energy, 193, (2022), 821-831.

Liu, Y., Wu, H., Wang, Y., Feng, G., Hu, A., Zhang, K., et al. A comparative analysis of flow channeling and heat extraction behavior between water- and ScCO2 -based Enhanced Geothermal Systems considering fracture aperture heterogeneity. Renewable Energy, 256, (2026).

Settgast, R. R., Aronson, R. M., Besset, J. R., Bui, Q. M., Byer, T. J., Castelletto, N., et al. GEOS: A performance portable multi-physics simulation framework for subsurface applications. Journal of Open Source Software, 9, (2024), 1-5.